

OH-bearing planar defects in olivine produced by the breakdown of Ti-rich humite minerals from Dabie Shan (China)

Jörg Hermann · John D. Fitz Gerald ·
Nadia Malaspina · Andrew J. Berry ·
Marco Scambelluri

Received: 14 August 2006 / Accepted: 23 October 2006 / Published online: 21 November 2006
© Springer-Verlag 2006

Abstract The partial breakdown of Ti-chondrodite and Ti-clinohumite during exhumation from ultra-high pressure to amphibolite facies conditions in garnet-pyroxenites from Dabie Shan (China) produces coronas of olivine coexisting with ilmenite blebs. Fourier transform infrared (FTIR) spectra of this newly formed olivine exhibit absorption bands in the hydroxyl-stretching region. Two intense peaks were observed at 3,564 and 3,394 cm^{-1} , identical in energy to peaks in Ti-clinohumite. Transmission electron microscopy (TEM) of the same olivine domains revealed the presence of a complex (001) planar intergrowth. These interlayers have a 1.35 nm repeat distance, which is characteristic of clinohumite. Such interlayers are also enriched in Ti with respect to the adjacent olivine as shown by energy dispersive spectrometry. The combined evidence from FTIR spectroscopy and TEM indicates that OH is incorporated along Ti-clinohumite planar defects. This study provides evidence that the nominally anhydrous phase olivine may contain OH as a humite-type defect

beyond the breakdown of the hydrous humite minerals and confirms earlier suggestions that Ti plays a key role in OH incorporation in mantle olivine. We suggest that olivine containing Ti-clinohumite defects is an important phase for water transport in subduction zones and for the storage of water in cold subcontinental mantle. However, these defects are unlikely to be stable in hotter parts of the oceanic mantle such as where basaltic magmas are generated.

Keywords Ti-chondrodite · Ti-clinohumite · OH in olivine · Transmission electron microscopy · Infrared spectroscopy · UHP metamorphism

Introduction

Significant amounts of water can be stored in the mantle in nominally anhydrous minerals (NAMs) such as olivine and pyroxenes (Bell and Rossman 1992). The incorporation mechanism of OH in mantle minerals is important for understanding a whole range of physical and chemical properties of the mantle including rheology, partial melting, diffusion, electrical conductivity, and seismic wave speeds and attenuation (Bell and Rossman 1992; Hirth and Kohlstedt 1996; Karato and Jung 1998). Previous studies have suggested that OH is associated with different types of defects in olivine. For example, Kitamura et al. (1987), Drury (1991) and Rissold et al. (2001) presented TEM evidence for planar defects associated with OH. The water content of olivine is most commonly determined from the intensity of absorption bands corresponding to hydroxyl stretching vibrations in infrared spectroscopy (Bell and Rossman 1992). Different energies of the absorption bands have

Communicated by J. Hoefs.

J. Hermann (✉) · J. D. Fitz Gerald · A. J. Berry
Research School of Earth Sciences,
The Australian National University,
Canberra, ACT 0200, Australia
e-mail: joerg.hermann@anu.edu.au

N. Malaspina · M. Scambelluri
Dipartimento per lo Studio del Territorio e delle sue
Risorse, University of Genova, 16132 Genova, Italy

Present Address:

A. J. Berry
Department of Earth Science and Engineering,
Imperial College London, London SW7 2AZ, UK

been attributed to different types of defects (Bai and Kohlstedt 1993; Lemaire et al. 2004). In a recent paper, Berry et al. (2005) showed that in order to reproduce the most common and intense hydroxyl stretching bands generally found in spinel peridotite olivine, the OH defect must be associated with the trace element Ti. Such a connection has also been proposed on the basis of Ti-solubility experiments in olivine (Hermann et al. 2005). Further, lamellae of Ti-clinohumite in olivine have been identified by Wirth et al. (2001) who used TEM to characterise olivine reaction products in a synthetic lherzolite, containing H₂O and TiO₂, that had been equilibrated at 8 GPa and 1,300°K for 24 h.

In this paper we use a natural system to study the incorporation of water in olivine that results from the breakdown of Ti-clinohumite and Ti-chondrodite. These humite minerals have the general formula $nM_2SiO_4.M_{1-x}Ti_x(OH,F)_{2-2x}O_{2x}$, where x varies between 0 and 0.5 and $n = 4$ for clinohumite and $n = 2$ for chondrodite (Jones et al. 1969). In ultramafic rocks, the M cation corresponds mainly to Mg with subordinate Fe and Ni. Olivine and the humite minerals may be

regarded as a polysomatic series (Thompson 1978) with the endmembers norbergite ($n = 1$) and olivine ($n = \text{infinity}$). The humite breakdown reactions must be related to the release of an aqueous fluid since the reactants contain 0.5–2 wt% H₂O whereas the products, olivine and ilmenite, are nominally anhydrous minerals. This ensures a H₂O- and Ti-rich environment at the time of olivine formation. Such conditions are ideal for determining the type of defects that form in olivine and whether or not there is a link between Ti and OH incorporation. In this study we use petrography, petrology, TEM and FTIR to characterise OH bearing defects in olivine and the environment in which they formed.

Sample description and petrography

We have investigated in detail a Ti-chondrodite and Ti-clinohumite bearing garnet-pyroxenite that outcrops in the Maowu ultramafic complex of the Central Dabie ultra-high pressure (UHP) metamorphic unit in Dabie

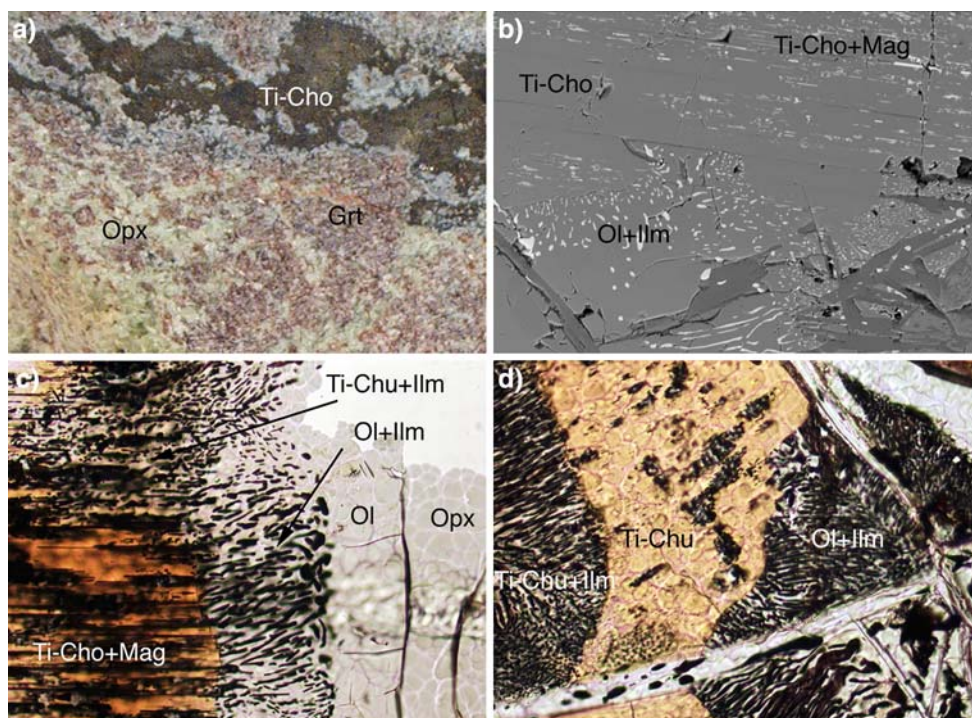
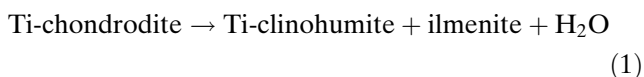


Fig. 1 **a** Hand specimen image of a garnet orthopyroxenite (*Grt* garnet, *Opx* orthopyroxene) with a layer consisting of Ti-chondrodite (*Ti-Cho*) and Ti-clinohumite. Field of view is 4 cm. **b** Back scatter electron image of an olivine (*Ol*) corona, showing vermicular intergrowth with ilmenite (*Ilm*), around Ti-chondrodite containing oriented magnetite (*Mag*) lamellae. Field of view is 400 μm . **c** Transmitted light photomicrograph of the reaction texture between Ti-chondrodite with magnetite lamel-

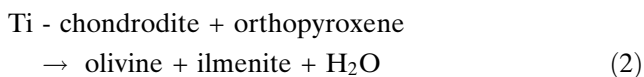
lae and an orthopyroxene inclusion containing olivine domains with and without ilmenite blebs. A small area with Ti-clinohumite (*Ti-Chu*) plus ilmenite replaces former Ti-chondrodite. Field of view is 170 μm . **d** Transmitted light photomicrograph of a composite corona around Ti-chondrodite (to the left, outside the view of the picture) consisting of Ti-clinohumite + ilmenite, clean Ti-clinohumite and olivine + ilmenite. Field of view is 280 μm

Shan (China). This body consists of layered mafic/ultramafic rocks ranging from harzburgites to orthopyroxenites, associated with coesite-eclogites, and hosted by garnet-coesite-bearing gneisses (Liou and Zhang 1998). Peak metamorphic conditions of 4.0 ± 1.0 GPa and $700 \pm 50^\circ\text{C}$ have been determined previously (Liou and Zhang 1998; Jahn et al. 2003).

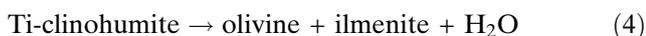
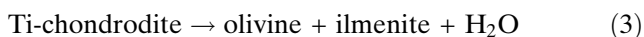
The selected sample (171) displays an assemblage dominated by orthopyroxene and garnet, with minor clinopyroxene. Accentuated dark layers host the great majority of the Ti-rich humites (Fig. 1a). In thin section, coarse, poikiloblastic orthopyroxene and garnet with polyphase solid inclusions are common. These features have been described in detail by Malaspina et al. (2006), who concluded that such orthopyroxenites originate from metasomatism close to peak metamorphic conditions by the interaction of felsic silicate melts, sourced from the adjacent gneisses, with ultramafic lenses that contain Ti-humite minerals. Ti-chondrodite grains display equilibrium textures with garnet, clinopyroxene and orthopyroxene indicating that Ti-chondrodite was a stable phase at peak metamorphism. The first clear textural evidence for partial breakdown is observed at the border of large grains of Ti-chondrodite, where clusters of Ti-clinohumite form that contain irregular blebs of ilmenite (Fig. 1d). This texture suggests a partial breakdown of Ti-chondrodite according to the generalised reaction:



At the grain boundaries between orthopyroxene and Ti-chondrodite a composite olivine corona has been observed. Adjacent to orthopyroxene, ~ 100 μm wide clear olivine bands form whereas adjacent to Ti-chondrodite, slightly wider bands consisting of olivine and ilmenite are present (Fig. 1c). These observations suggest a second type of reaction:



The most common feature is a discontinuous rim of olivine, up to 200 μm wide, that contains numerous blebs of ilmenite surrounding Ti-chondrodite and Ti-clinohumite (Fig. 1 b, d). This texture is related to the generalised partial breakdown reaction of the Ti-rich humites:



It is worth noting that complete breakdown of the Ti-rich humites is not observed. Hence the major part of the evolution of these rocks must have occurred in a field where olivine, ilmenite and humite minerals were stable. Isolated serpentine and chlorite veins document retrogression at low-grade metamorphic conditions.

Ti-chondrodite also contains numerous oriented magnetite lamellae (Fig. 1b, c). In regions where Ti-chondrodite is replaced by Ti-clinohumite, a few “ghost” magnetite lamellae are incorporated in the Ti-clinohumite (Fig. 1c). On the other hand, newly formed Ti-clinohumite and olivine (Fig. 1d) do not contain magnetite. These observations indicate that the magnetite exsolution most likely occurred prior to the partial breakdown of Ti-chondrodite. We suggest that these magnetite lamellae formed by partial oxidation of Ti-chondrodite close to peak conditions. The infiltration of a hydrous silicate melt, which reacted with olivine to form the orthopyroxenite (Malaspina et al. 2006), might have been the oxidising agent.

Analytical techniques

Major and minor element compositions of minerals were determined by wavelength dispersive spectrometry using a Cameca SX 100 electron microprobe at the Research School of Earth Sciences. The acceleration voltage was set to 15 kV, the beam current to 20 nA and counting times varied between 10 and 40 s. Natural and synthetic silicates, oxides and metals were used for standardisation. Mineral analyses were complemented by detailed back scattered electron (BSE) images to enable grains from the desired microtextural relationship to be selected.

TEM imaging, diffraction and analysis was carried out at 300 kV using a Philips CM300T with a LaB₆ filament, a Gatan 794 multi-scan CCD camera and an EDAX super-ultra-thin-window Si(Li) X-ray detector. Grids glued to double polished petrographic sections of ~ 40 μm thickness were prepared for TEM using an Ar-ion beam thinner. Fourier transform infrared (FTIR) spectra were recorded using a Bruker A590 infrared microscope attached to a Bruker IFS28 infrared spectrometer. The system uses a globar source and liquid nitrogen cooled MCT detector. The spectra reported are unpolarised, have a resolution of 2 cm^{-1} , and represent the average of 256 scans. The entire light path was purged with dry N₂ to remove atmospheric water vapour. Infrared spectra were recorded from the same samples as used for the TEM analyses. The double polished wafer varied in thickness from 40 μm outside

the areas thinned with the ion beam to $\sim 10 \mu\text{m}$ close to the areas analysed by TEM. Spectra were obtained from spots with a $50 \mu\text{m}$ diameter by using an aperture. This is essential to spatially discriminate between humite minerals and nominally anhydrous phases such as olivine and orthopyroxene.

Mineral compositions

Orthopyroxene and clinopyroxene have high $\text{Mg}_{\#}$ (93–94) and garnet is pyrope-rich (70–73%). Low CaO (0.03–0.09 wt%) and Al_2O_3 (<0.1 wt%) contents of orthopyroxene coexisting with clinopyroxene and garnet are consistent with the previous P – T estimates of $4.0 \pm 1.0 \text{ GPa}$ and $750 \pm 50^\circ\text{C}$ (Liou and Zhang 1998). Ti-chondrodite is characterised by high TiO_2 (5–7 wt%) and high F (1.3–2.2 wt%) contents (Table 1). These values translate into 0.24–0.32 Ti cations per formula unit (pfu) and 0.25–0.41 F pfu, when normalised to seven cations. The high $\text{Mg}_{\#}$ (91–93) and high NiO (0.43–0.66 wt%) contents of chondrodite support

Table 1 Representative electron microprobe analyses of Ti-chondrodite (Ti-Cho), Ti-clinohumite (Ti-Chu) and olivine (Ol)

	Ti-Cho	Ti-Chu	Ol
SiO_2	34.04	36.36	40.82
TiO_2	5.27	4.29	0.19
Al_2O_3	0.00	0.00	0.01
Cr_2O_3	0.12	0.03	0.00
FeO	7.24	7.65	8.98
MgO	49.61	49.53	49.98
MnO	0.05	0.06	0.06
CaO	0.00	0.00	0.01
NiO	0.49	0.66	0.81
F	1.75	0.50	–
H_2O	1.11	0.67	–
Total	98.95	99.53	100.87
Norm	7	13	3
Si	2.010	3.925	0.990
Ti	0.234	0.348	0.004
Al	0.000	0.000	0.000
Cr	0.006	0.003	0.000
Fe	0.358	0.691	0.182
Mg	4.368	7.971	1.807
Mn	0.003	0.005	0.001
Ca	0.000	0.000	0.000
Ni	0.024	0.057	0.016
F	0.328	0.169	0.000
OH	0.439	0.483	0.000
XMg	0.924	0.920	0.908

The compositions were normalised to 7, 13 and 3 cations, respectively. All Fe is treated as FeO. H_2O was calculated on the basis of the measured F and Ti contents using the exchange vectors $\text{Ti}_x\text{O}_{2x}\text{M}_{1-x}(\text{OH})_{2-2x}$ and OH-F_{-1} . Totals take the substitution of F for O into consideration

an ultramafic origin. Ti-clinohumite displays the same NiO content and high $\text{Mg}_{\#}$ as Ti-chondrodite but lower TiO_2 (4.3–4.8 wt%; 0.35–0.40 Ti pfu when normalised to 13 cations) and F (0.4–0.8 wt%; 0.13–0.26 F pfu) values. Olivine has a $\text{Mg}_{\#}$ of 91, high NiO contents of 0.8 wt% and detectable TiO_2 that varies from 0.02 to 0.2 wt%. Elemental analyses of orthopyroxene, clinopyroxene and garnet are given in Malaspina et al. (2006).

TEM observations

An elongate orthopyroxene grain surrounded by a single large chondrodite grain was selected for characterisation by TEM. Part of the ion-thinned region is shown in Fig. 1c. The complex zone between the orthopyroxene and chondrodite, containing several grains of olivine intergrown with clinohumite and ilmenite, was studied in detail.

Ilmenite blebs show no crystallographic relationship with the surrounding olivine. Clinohumite lamellae, on the other hand, show a clear relationship. With refer-

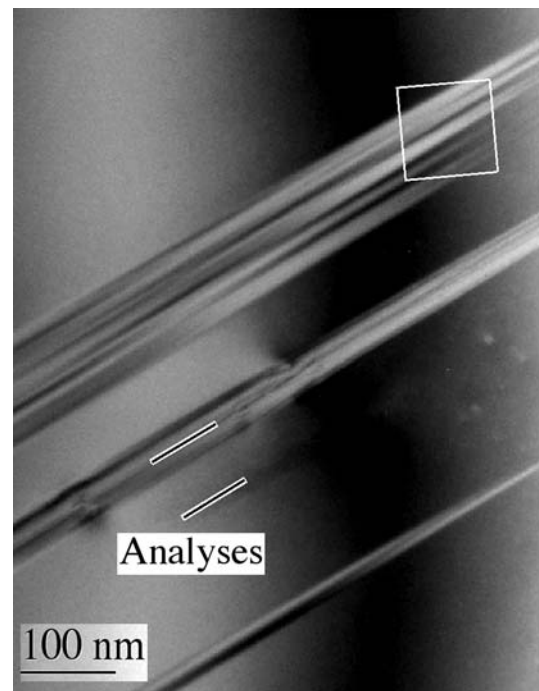


Fig. 2 Bright-field TEM micrograph of an olivine region from the ion-thinned foil of the sample shown in Fig. 1c. The olivine was oriented in this image with its [b] axis within $\sim 2^\circ$ of the electron beam. Crossing the olivine crystal are three groups of fringes, characteristic of planar defects; each planar defect is parallel to olivine (001). The lines labelled “Analyses” correspond to the regions from which the TEM-EDS spectra were recorded

ence to the common space groups for olivine (Pbnm) and Ti-clinohumite ($P2_1/b$), the lamellae are oriented parallel to $(001)_{Ol}$, with

$$(001)_{Ol} \parallel (001)_{Ti-Chu}$$

$$[010]_{Ol} \parallel [010]_{Ti-Chu}$$

where Ol = olivine and Ti-Chu = Ti-clinohumite.

Figure 2 is a TEM image of olivine with lamellae viewed near to the common $[010]$ -axis. Figure 3a shows the (001) lamellae in more detail in the form of the $[010]$ -zone-axis lattice image. Figure 3b is an enlargement of a small area in 3a revealing the regular repeat of the olivine unit cells at the top and bottom of the frame with 4 units of a longer-period structure in the centre. The repeat distance of 1.35 nm is characteristic of the (001) plane spacing of clinohumite.

‘Qualitative’ X-ray analyses were also carried out using the TEM, taking advantage of the very small analysis spot achievable with this type of instrument. Unfortunately quantitative measurements could not be made with an electron beam small enough to only analyse the thin lamellae; instead a beam 20 nm wide and 60 nm long was aligned with its long axis parallel to the lamellae. The two spectra in Fig. 4 were collected on the lamella and on the adjacent olivine approximately at the positions indicated in Fig. 2. Peaks in the spectra due to the major elements in the two regions analysed are indistinguishable. However, as revealed in the enlarged segment of Fig. 4, Ti is undetectable in the olivine-only region but is clearly

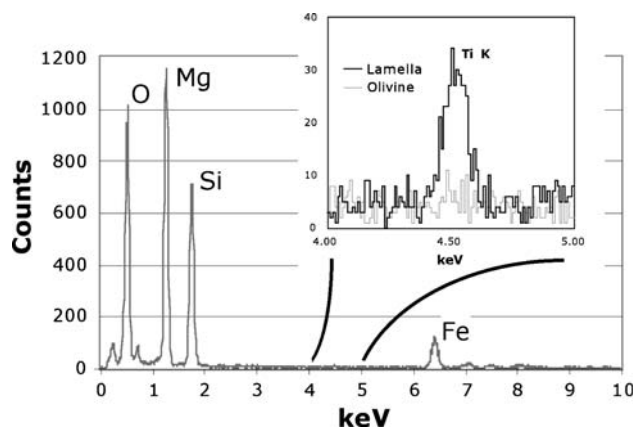


Fig. 4 TEM-EDS spectra of the two regions indicated by the ‘Analyses’ lines in Fig. 2. A group of lamellae and adjacent defect-free olivine were analysed with an elongated 60×20 nm electron beam. The major element counts in the two regions are indistinguishable. In contrast, the inset shows the spectra in the 4–5 KeV region where the lamellae clearly exhibit a Ti peak, which is absent for the olivine host

present in the lamella, consistent with them being Ti-clinohumite.

Some preference was noted for the olivine closest to the orthopyroxene to contain the fewest (001) lamellae, with lamellae being completely absent in some cases. Close to the Ti-chondrodite and where ilmenite blebs are present, all the olivine contains lamellae though the density varies locally. Some regions in the reacted zone contain layers of Ti-clinohumite up to 500 nm thick. Where intergrown with olivine, these

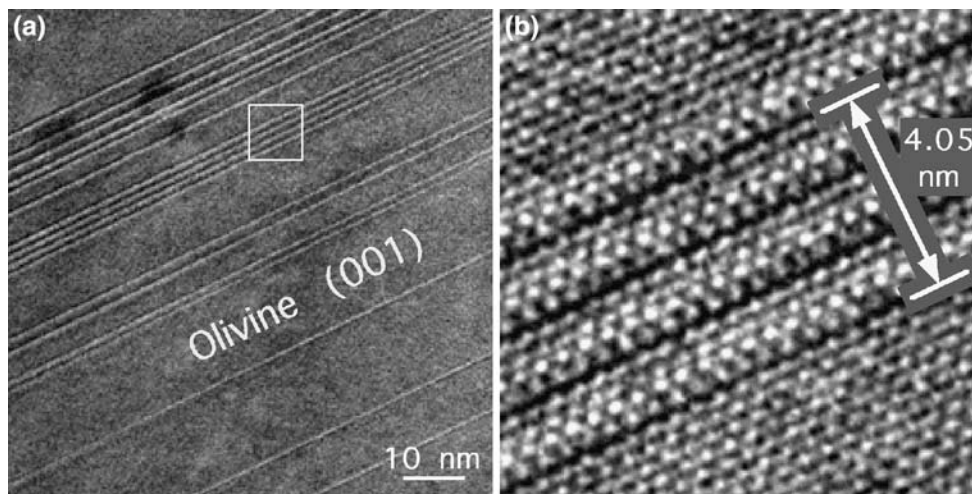


Fig. 3 Detail of the region marked by the box in Fig. 2, but now with its crystallographic $[b]$ axis carefully aligned parallel to the electron beam of the TEM. **a** Clearly shows a complex pattern of (001) planar defects. **b** At much higher magnification of the region shown by the white box in **a**, the lattice image reveals the

regular repeat of the olivine unit cells (top and bottom of image) plus 4 units of a longer-period structure across the centre of the image. The width of three such layers is 4.05 nm, yielding a 1.35 nm repeat distance characteristic of clinohumite

layers maintain the crystallographic relationship identified above (composite [010] diffraction pattern identical to that of Fig. 8 from Wirth et al. 2001), and Ti signals were easily detectable using EDX. Careful note was taken of the location and extent of these regions as the basis for some of the FTIR spectroscopy discussed in the following section.

Intergrowths in the Ti-chondrodite (Cho) regions of the thin foil were also examined by TEM. The plane of magnetite (Mt) lamellae was identified as $(111)_{Mt}$ with $(111)_{Mt} \parallel (100)_{Cho}$. In places, chondrodite has also converted to olivine with $[100]_{Ol} \parallel [100]_{Cho}$ and inherited intact $(111)_{Mt}$ lamellae, which therefore lie parallel to $(100)_{Ol}$. This olivine also shows ilmenite blebs and occasional (001) lamellae that are much thinner and presumably identical to those described above.

FTIR spectroscopy

The ion-beam thinned TEM sample is ideal for studying OH-rich minerals such as humites by FTIR because the short path-length allows transmission spectra to be recorded for the strongly absorbing OH stretching region. Ti-chondrodite contains intense characteristic peaks in this region at 3,384 and 3,564 cm^{-1} (Fig. 5a,b). A minor peak was observed at 3,525 cm^{-1} and weak peaks are present at $\sim 3,325$ and $\sim 3,415$ cm^{-1} , which result in a broadening of the main peak at 3,384 cm^{-1} . Ti-clinohumite displays identical peaks to Ti-chondrodite at 3,564 and 3,525 cm^{-1} . However, the main peak is shifted to higher energy and occurs at 3,394 cm^{-1} (Fig. 5d–f). This distinction between Ti-clinohumite and Ti-chondrodite on the basis of their IR-spectra was earlier documented by Matsyuk and Langer (2004). Ti-clinohumite grains containing ilmenite inclusions and inclusion-free Ti-clinohumite as shown in Fig. 1d, display very similar IR spectra (Fig. 5e,f). Also, Ti-clinohumite adjacent to Ti-chondrodite, and derived from its breakdown, produces the same spectrum (Fig. 5d). The only small difference in all the recorded Ti-clinohumite spectra is the variable intensity of the minor peak at 3,525 cm^{-1} , which is attributed to differences in the orientation of the analysed grains. Clean olivine bordering orthopyroxene and olivine containing numerous ilmenite blebs were also analysed (Fig. 1c). Both types of olivine display peaks at 3,564 and 3,394 cm^{-1} , identical in energy to those observed for Ti-clinohumite. Olivine bordering Ti-chondrodite (Fig. 5a) displays the peak at 3,394 and not at 3,384 cm^{-1} , indicating that the OH signal does not derive from accidental analysis of Ti-chondrodite, but represents OH incorporated in

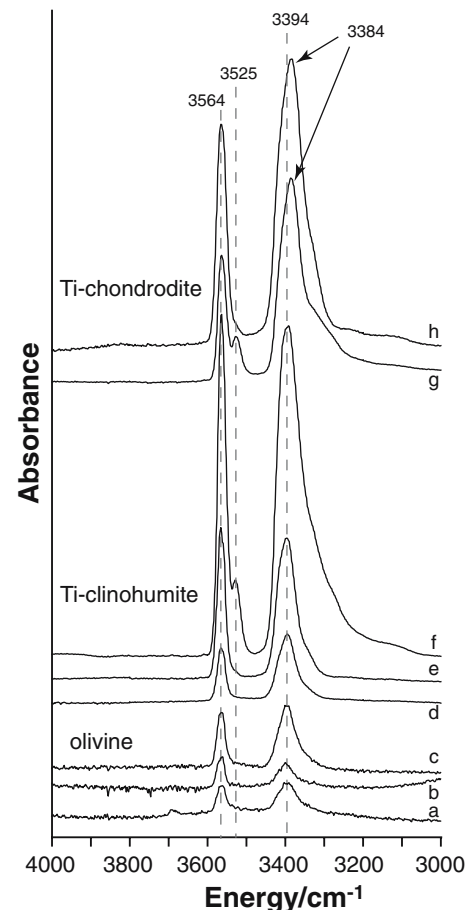


Fig. 5 Unpolarized FTIR spectra of olivine, Ti-clinohumite and Ti-chondrodite. The thickness of the analysed TEM foil varies influencing the relative absorbance. **a** Olivine with ilmenite and **b** ilmenite-free olivine with few and **c** abundant Ti-clinohumite interlayers as determined using TEM. **d** Ti-clinohumite (+ilmenite) replacing Ti-chondrodite. All four spectra were recorded from the field of view of Fig. 1c. **e** Corona of Ti-clinohumite + ilmenite and **f** clean Ti-clinohumite as shown in Fig. 1d. **g** Ti-Chondrodite spectra from the region where spectra (a–d) were taken and (**h**) from the grain that has the corona of Ti-clinohumite (region of spectra e and f). Note that there is a shift in the main peak from 3,384 cm^{-1} in Ti-chondrodite to 3,394 cm^{-1} in Ti-clinohumite

olivine. In the clear olivine, we have analysed spots in regions with high and low densities of planar defects as identified by TEM (Fig. 5b, c). The area of the hydroxyl absorption in the spectra is a function of sample thickness and water content. The thickness of the sample in the two analysed regions is comparable and hence the intensity of absorption is related to the amount of OH. The observed spectra indicate that the region with higher density of defects contains significantly higher OH. Orthopyroxene adjacent to the clear olivine (Fig. 1c) displays no absorption in the hydroxyl-stretching region.

Discussion

Stability of humite minerals in UHP rocks

Detailed textural investigations of a Ti-chondrodite and Ti-clinohumite bearing garnet-pyroxenite from the Central Dabie Shan UHP complex indicate that Ti-chondrodite is in textural equilibrium with peak metamorphic garnet and orthopyroxene, whereas Ti-clinohumite forms at the edges of Ti-chondrodite grains as the product of a partial recrystallisation. Ti-chondrodite is occasionally included in orthopyroxene that forms during metasomatism close to peak metamorphic conditions, indicating that Ti-chondrodite was already present during the prograde evolution of the rocks (Malaspina et al. 2006). In the following discussion we will compare available experimental data on the stability of Ti-rich humites with the inferred P-T path of the Central Dabie Shan complex in order to evaluate whether the observed partial breakdown of the humite minerals is related to prograde or retrograde metamorphism (Fig. 6).

The significant amount of F in the humite minerals is important for understanding the textures and reactions that evolve during partial breakdown. F strongly enhances the stability field of humite minerals as has been demonstrated for both natural samples (Evans and Trommsdorff 1983; Lopez Sanchez-Vizcaino et al. 2005) and experimental compositions (Engi and Lindsley 1980; Weiss 1997). Consequently humite breakdown by reactions (2) and (3, 4) is continuous, and occurs in a field where all phases are present. The best experimental constraint is available for the breakdown of Ti-clinohumite with different compositions (Weiss 1997). In Fig. 6 the reaction for a F-free, Ti-saturated ($X = 0.5$) clinohumite is shown. The experiments further demonstrated that the addition of F shifts the breakdown of Ti-clinohumite to higher temperatures leading to a field where clinohumite is gradually transformed into olivine and ilmenite. This is in excellent agreement with the textural observations of small olivine rims around Ti-clinohumite and Ti-chondrodite. For the other reactions there are only limited experimental constraints. Stalder and Ulmer (2001) showed in a MgO–SiO₂–H₂O system (i.e. without Fe, Ti and F) that the assemblage clinohumite + orthopyroxene is restricted to high pressures >4 GPa. It is expected that in the presence of Ti and F the stability of clinohumite + orthopyroxene will be enlarged to lower pressures, but the general topology with olivine + ilmenite on the low pressure side will most likely remain unchanged. Finally, the experiments of Weiss (1997) have shown that in a fixed bulk

composition, Ti-chondrodite is stable to higher pressures for a given temperature than Ti-clinohumite, in agreement with our observed reaction (1).

Combining these experimental constraints with the textural observations and the inferred metamorphic evolution, it is evident that Ti-chondrodite was a stable phase at peak metamorphic conditions (Fig. 6). The partial break down of Ti-chondrodite to Ti-clinohumite (reaction 1) and the formation of new olivine + ilmenite (reactions 2, 3 and 4) at the expense of Ti-chondrodite and Ti-clinohumite is consistent with decompression of the rocks from UHP conditions to mid-crustal levels (Fig. 6). During this decompression, the stability field of F-free Ti-clinohumite is overstepped and its partial breakdown occurs in a divariant field where F–Ti clinohumite, olivine, ilmenite and an aqueous fluid are present. Interestingly, Ti-chondrodite does not completely react to Ti-clinohumite during this decompression. We suggest that the higher relative F content (F/OH = 0.75; Table 1) stabilises Ti-chondrodite with respect to Ti-clinohumite (F/OH = 0.35).

A very similar evolution has been described for Ti-clinohumite from the Su-Lu UHP terrane (Yang 2003). Yang (2003) suggested that the Ti-rich layers derive from a former Fe-Ti-gabbro that underwent severe Mg-metasomatism, as observed at lower metamorphic grade for gabbros enclosed in serpentinites (Scambelluri and Rampone 1999). The Ti-humite minerals studied here display high Mg_# and high Ni contents and are more likely to be related to an ultramafic protolith and may derive from Ti-clinohumite bearing veins, which are common in serpentinites (Trommsdorff and Evans 1980; Scambelluri et al. 1995).

Formation of humite lamellae in olivine

Crystal structure refinements of the humites, which have the general formula $nM_2SiO_4.M_{1-x}Ti_x(OH,F)_{2-2x}O_{2x}$, have demonstrated that Ti is incorporated in the interlayer by the exchange $TiO_2 \leftrightarrow Mg(OH)_2$ (Fujino and Takeuchi 1978). F can substitute directly for OH (Evans and Trommsdorff 1983). As there are twice as many $M_{1-x}Ti_x(OH,F)_{2-2x}O_{2x}$ layers in chondrodite as in clinohumite with respect to the M_2SiO_4 units, there is a higher potential to incorporate Ti and also F in chondrodite (Table 1). The analysed Ti-chondrodite and Ti-clinohumite contain significantly less OH than the hydroxyl endmember compositions because the presence of Ti and F both reduce the amount of OH (Berry and James 2002). Nevertheless, the calculated structural formula provides evidence that both phases still contain a significant amount of OH.

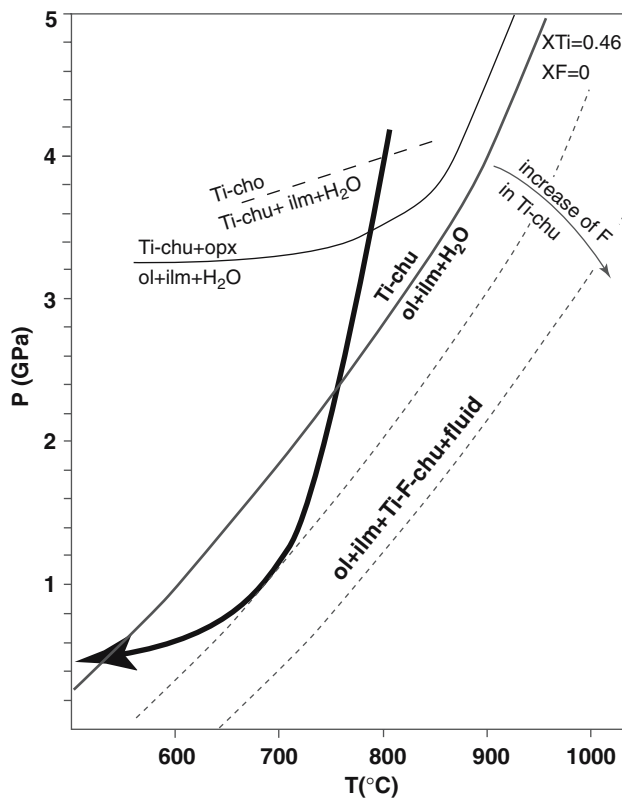


Fig. 6 Schematic retrograde P - T path of the Maowu rocks (**bold arrow**; after Liou and Zhang 1998) compared to the experimentally determined stability field of OH-Ti-clinohumite (Weiss 1997; Ulmer and Trommsdorff 1999). The incorporation of F in Ti-clinohumite increases its stability field (schematically shown with the *dashed lines*) and results in a divariant field, where F-Ti-clinohumite, olivine, ilmenite and an aqueous fluid are stable. Abbreviations as in Fig. 1

Consequently, the reaction from Ti-chondrodite to Ti-clinohumite (1) will liberate some H_2O as the number of hydrous interlayers decreases. Reactions (2) and (3) have hydrous phases on the reactant side and anhydrous minerals on the product side, and must also liberate H_2O . Hence the olivine derived from these reactions formed in the presence of ilmenite and an aqueous fluid. TEM investigation of such newly formed olivine reveals the presence of planar defects. These defects are oriented along the (001) plane of olivine and display a 1.35 nm repeat distance as is typical for clinohumite (Robinson et al. 1973; Risold 2001). Local EDS in zones with a large density of such defects showed clear evidence of increased Ti contents. The 20×60 nm elongate-beam analysis in the TEM (Fig. 4) is known to have included regions of both Ti-clinohumite defect lamellae + olivine. The non-trivial calculation of convoluting the electron beam profile with the size and shape of such clinohumite lamellae embedded in a matrix of olivine was not attempted,

hence the spectra shown are strictly qualitative in nature. Nevertheless, the Ti signal level measured here, adjusted for the proportions of olivine-clinohumite in the analysed region, was broadly consistent with that recorded from thicker clinohumite layers, indicating that the Ti content is constant in the clinohumite regardless of the stacking thickness. Also, FTIR-spectroscopy of lamellae-rich olivine provides evidence for hydroxyl-stretching at energies identical to those observed in Ti-clinohumite. These observations indicate that the partial breakdown reactions of Ti-chondrodite (3) and Ti-clinohumite (4) to olivine are transitional with decreasing numbers of $M_{1-x}Ti_x(OH,F)_{2-2x}O_{2x}$ interlayers produced as the reaction progresses. This observation can be neatly described in terms of a polysomatic series with the endmembers norbergite ($n = 1$) and olivine ($n = \text{infinity}$). This means that there is an increasing number of olivine units present (increasing n) for each hydrous interlayer during the partial breakdown of the humite minerals.

In summary, dehydration reactions such as (3) and (4) do not liberate H_2O in a single pulse for two reasons. Firstly, the solid solution of Fe, Ti and F in humites results in a multivariant field, where all phases involved in the reaction are stable and where dehydration is continuous. Secondly, the nominally anhydrous phase olivine contains planar humite type defects, which continue to dehydrate outside the stability field of the humite minerals. These observations provide an important link between FTIR-spectroscopy, mineral chemistry and mineral defects at an atomic scale and identify a mechanism of OH incorporation in olivine.

The olivine/clinohumite crystallographic relationship

In this study we have used the space group Pbnm for olivine and $P2_1/b$ for clinohumite because the lattice dimensions of the two minerals are then directly comparable (Ribbe 1980). TEM investigation revealed that the orientation of the (001) lamellae in olivine is:

$$(001)_{Ol} \parallel (001)_{Ti-Chu}$$

$$[010]_{Ol} \parallel [010]_{Ti-Chu}$$

The orientations we have established appear at first glance to be different to those of the lamellae observed by Wirth et al. (2001) who reported planes parallel to (001)_{Ol} and

$$[100]_{Ol} \parallel [100]_{Ti-Chu}$$

$$(001)_{Ol} \parallel (001)_{Ti-Chu}$$

$$(020)_{Ol} \parallel (020)_{Ti-Chu}$$

However, these relationships require correction and the true crystallographic orientation of the lamellae in

Wirth et al.'s experimentally produced materials is identical to that established here for the Dabie Shan samples.

Wirth et al. (2001) pointed out the possibility of “confusion regarding the crystal setting” arising from the common selection of the $P2_1/b$ space group (unique axis **c**) for the monoclinic humite minerals (the alternative setting is $P2_1/c$ with unique axis **b**). Unfortunately, Wirth et al. (2001) added to the confusion through an error in their data Table 1: their a, b and c cell dimensions are correct for the $P2_1/b$ setting, but the obtuse Ti-clinohumite monoclinic cell angle of 101° , labelled as β , should be α .

Correction of their cell angle error invalidates the crystallographic inter-relationship. The interplanar angle $(020) \wedge (001)$ for Ti-clinohumite in the $P2_1/b$ setting is $\alpha^* = 79^\circ$, yet the angle $(020) \wedge (001)$ for orthorhombic olivine is of course 90° , therefore (001) and (020) parallelism between the two minerals is impossible.

The $[010]$ diffraction pattern shown in Fig. 8 of Wirth et al. (2001) should also be corrected. The label for a^* of Ti-clinohumite needs to be added to this pattern, parallel to a^* of olivine, since $[010]$ of the two phases are clearly parallel.

Finally, we note that the clinohumite–olivine crystallographic relationship we describe here is totally consistent with the atomic similarities emphasised for this family of minerals by Ribbe (1980) and clearly illustrated on the left side of Ribbe's Fig. 1.

Other occurrences of humite lamellae in olivine

In this section, we summarise occurrences of Ti-clinohumite lamellae in olivine and compare the inferred conditions of formation in order to constrain the parts of the upper mantle where such defects might be significant.

Humite lamellae in olivine were first described from “orange grains” in the Buell Park kimberlite, Arizona (Kitamura et al. 1987). These authors provided TEM images of planar defects and noticed the similarity of the FTIR spectra of the olivine with Ti-clinohumite. In fact, the spectral signature (energy and intensity) of the Buell Park olivine is essentially identical to the peaks observed for olivine with Ti-clinohumite lamellae reported here. The estimated conditions of formation are $1,000^\circ\text{C}$ and $\sim 2\text{--}3$ GPa and both Ti-clinohumite and Ti-chondrodite occur in the same kimberlite (Aoki et al. 1976). Drury (1991) showed TEM images of planar defects on dissociated dislocations in olivine from the Erro-Tobbio peridotite (Voltri Massif, Western Alps) and attributed their formation to retrograde

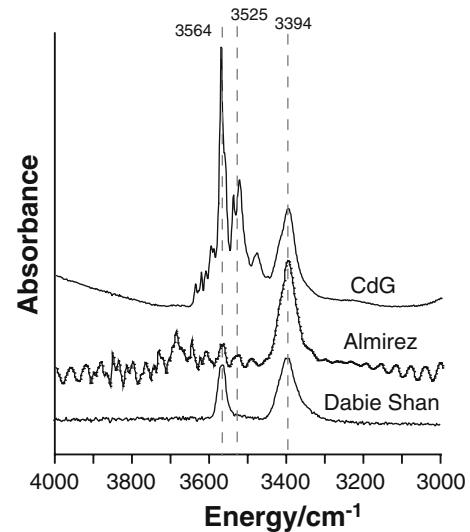


Fig. 7 Unpolarized FTIR spectra of olivine from the Dabie Shan (China) orthopyroxenite presented in Fig. 5c, from an olivine-orthopyroxene fels (Almiraz massif, Spain) and from a garnet peridotite (Cima di Gagnone, Switzerland). Note that all spectra display a strong OH-peak at $\sim 3,400$ cm^{-1} characteristic of Ti-clinohumite planar defects. The Almiraz spectrum displays interference fringes and a small contribution from atmospheric water

hydration in the amphibole peridotite field. No infrared analyses of these samples are available and P-T conditions are poorly constrained. The clearest TEM evidence for clinohumite lamellae in olivine has been provided by Risold et al. (2001) for garnet peridotites from Cima di Gagnone, Central Alps. These rocks were subducted during the Alpine orogeny and reached peak conditions of 740°C and 3 GPa (Nimis and Trommsdorff 2001). Also from this locality, relics of Ti-clinohumite have been described that contain significant amounts of F (Evans and Trommsdorff 1983). Figure 7 shows an IR spectrum we recorded from an olivine sample from Cima di Gagnone (Berry et al. 2005) that derives from the sample set investigated by Risold et al. (2001). It shows the characteristic peaks at $\sim 3,400$ cm^{-1} and $3,564$ cm^{-1} , which in the present study we attribute to the presence of Ti-clinohumite layers. Because olivine displays a number of OH absorbance bands within the energy range of $3,600\text{--}3,500$ cm^{-1} (Berry et al. 2005), the $3,564$ cm^{-1} peak may not always be diagnostic of Ti-clinohumite layers. In contrast, the $\sim 3,400$ cm^{-1} peak, which occurs at an energy where no other olivine-related OH peaks appear to occur, provides an excellent fingerprint for the presence of Ti-clinohumite layers in olivine. The Cima di Gagnone olivine grains also contain palisades of ilmenite rods that are aligned with the Ti-clinohumite layers. Risold et al. (2001) interpreted these rods

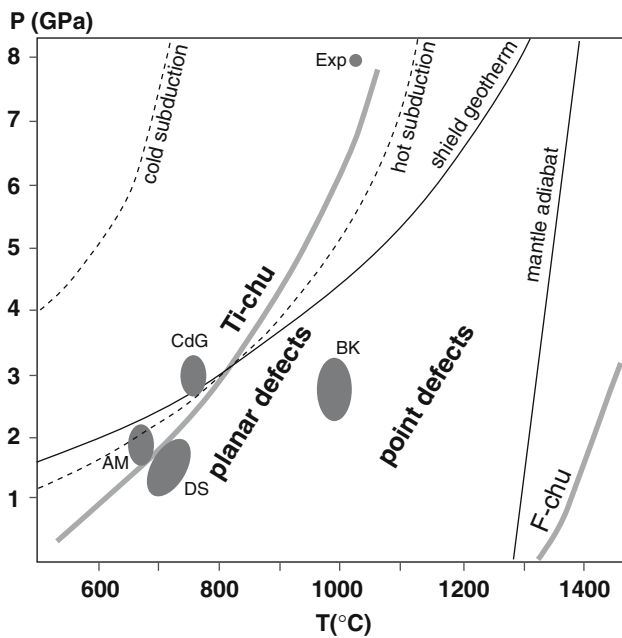


Fig. 8 Compilation of P - T conditions of olivine that display planar defects. *DS* Dabie Shan, *BK* Buell Park kimberlite, *CdG* Cima di Gagnone, *AM* Imirez Massif, *Exp* experimental result of Wirth et al. (2001). The breakdown curves of Ti-saturated F-free Ti-clinohumite and F-clinohumite are taken from Weiss (1997) and are also reported in Ulmer and Trommsdorff (1999). The P - T regions encountered in subduction environments (Kincaid and Sacks 1997), a typical shield geotherm corresponding to a heat flow of 40 mW/m^2 (Green and Falloon 1998) and a mantle adiabat with a potential temperature of $1,280^\circ\text{C}$ (McKenzie and Bickle 1988) are also shown

as resulting from the partial breakdown of the Ti-clinohumite layers to olivine + ilmenite + H_2O , with the alignment parallel to $(001)_{\text{OI}}$ seemingly being restricted to the break down of defect Ti-clinohumite layers. When grains of Ti-clinohumite break down, a vermicular intergrowth of olivine and ilmenite is observed (Trommsdorff and Evans 1980), in agreement with the textural observations in this study. Complex intergrowth textures between olivine, Ti-clinohumite and ilmenite have been reported recently from the Almirez Massif in Spain, where newly grown olivine formed during the high-pressure breakdown of antigorite serpentinite to olivine-orthopyroxene-chlorite peridotites at $\sim 670^\circ\text{C}$, 1.8 GPa (Lopez Sanchez-Vizcaino et al. 2005). These authors found that F-bearing Ti-clinohumite is an accessory phase in these rocks and that in some cases newly formed olivine contained lamellae of Ti-clinohumite that are visible in the optical microscope. Figure 7 shows an FTIR spectrum of olivine from these rocks. Again the characteristic peak of Ti-clinohumite lamellae in olivine at $\sim 3,400 \text{ cm}^{-1}$ is present. Finally, Ti-clinohumite lamellae in olivine that coexists with Ti-chondrodite and Ti-clinohumite have

been experimentally produced at 8 GPa and $1,027^\circ\text{C}$ by Wirth et al. (2001).

The inferred P - T conditions of these occurrences are plotted in Fig. 8 and compared to the experimentally derived stability field of Ti-clinohumite determined by Weiss (1997) and summarized by Ulmer and Trommsdorff (1999). The data provides strong evidence that Ti-clinohumite planar defects in olivine occur at conditions close to the breakdown of Ti-clinohumite and Ti-chondrodite.

Implications

Although in the studied samples humite breakdown is related to near-isothermal decompression, it can be used as a proxy for what happens when the humite stability field is overstepped during prograde subduction. In subduction zones, olivine with Ti-clinohumite planar defects might transport water into the mantle beyond the stability fields of the humite minerals (Fig. 8). Also, it is expected that such defect-rich olivine will have a different (weaker) rheology than normal mantle olivine, with consequences for deformation within the subducted slab and hydrous parts of the overlying mantle wedge (Kitamura et al. 1987; Drury 1991; Hirth and Kohlstedt 1996). Olivine with Ti-clinohumite planar defects also contains significantly higher Ti contents than defect-free olivine, and partial breakdown of such interlayers is able to produce ilmenite rods within olivine. These rods have been interpreted previously to form at extreme depths during decompression from the wadsleyite to olivine stability fields (Dobrzhinetskaya et al. 1996; Green et al. 1997). The present study demonstrates that Ti-rich clinohumite lamellae in olivine can form at moderate pressures. Additionally the dehydration breakdown of these $\text{Mg}_{0.5}\text{Ti}_{0.5}(\text{OH})\text{O}$ interlayers explains why the exsolved Ti phase in olivine is ilmenite rather than spinel. Therefore, this study supports the conclusions of Risold et al. (2001): ilmenite rods are the result of the breakdown of isolated Ti-clinohumite layers within olivine and hence cannot be used as indicators of extreme pressures.

The subcontinental mantle in cratons is a second environment where layered defects in olivine are likely to be of importance. A typical shield geotherm of 40 mW/m^2 crosses the F-free Ti-clinohumite stability field at $\sim 3 \text{ GPa}$. As the layered defects are stable beyond this break down curve (Fig. 8) we suggest that layered defects might occur in subcontinental mantle at significantly higher pressures. However, from the presented data it seems unlikely that such defects play an important role in the much hotter sub-oceanic mantle

and the formation of basalts. The mantle adiabat for a potential temperature of 1,280°C is far removed from the inferred stability of layered defects. Experiments have shown that OH defects in olivine at such high temperatures are still associated with Ti, but as a point-rather than a layer-type defect (Berry et al. 2005). From these observations we propose a progressive decrease of OH in olivine along the transition from hydrous humite-mineral grains to planar defects to point defects and finally to anhydrous olivine at very high temperatures as schematically shown in Fig. 8.

Conclusions

1. Ti-clinohumite defects parallel to (001) in olivine, as observed by TEM, display characteristic IR bands at $\sim 3,400\text{ cm}^{-1}$ and $3,564\text{ cm}^{-1}$. The $\sim 3,400\text{ cm}^{-1}$ band occurs in an energy region where olivine has no other OH-related absorbance peaks. This band can therefore be used in future studies to conveniently establish the existence of planar Ti-clinohumite defects in olivine even if TEM characterisation is not available.
2. The presence of both Ti and OH in interlayers provides evidence for a strong link between Ti and OH incorporation.
3. Planar Ti-clinohumite-like defects in olivine are able to store OH beyond the breakdown of humite minerals, indicating that such defects might be important for storing water in the cold subcontinental mantle and transporting water to great depths in subduction zones. This type of defect has only been observed previously in rocks that experienced conditions close to the stability field of OH-Ti-clinohumite and OH-Ti-chondrodite.

Acknowledgments We thank the Australian Research Council for financial support and Tom Sharp for his encouragement in the early stages of this work. N. Malaspina and M. Scambelluri acknowledge funding by the Italian MIUR-Cofin. We thank B. Evans and Stalder R for constructive comments and J. Hoefs for expeditious handling of the manuscript.

References

- Aoki K, Fujino K, Akaogi M (1976) Titanochondrodite and titanoclinohumite derived from the upper mantle in the Buell Park kimberlite, Arizona, USA. *Contrib Mineral Petrol* 56:243–253
- Bai Q, Kohlstedt DL (1993) Effects of chemical environment on the solubility and incorporation mechanism for hydrogen in olivine. *Phys Chem Minerals* 19:460–471
- Bell DR, Rossman GR (1992) Water in Earth's mantle: the role of nominally anhydrous minerals. *Science* 255:1391–1397
- Berry AJ, Hermann J, O'Neill HSC, Foran GJ (2005) Fingerprinting the water site in mantle olivine. *Geology* 33:870–873
- Berry AJ, James M (2002) Refinement of hydrogen positions in natural chondrodite by powder neutron diffraction: implications for the stability of humite minerals. *Mineral Mag* 66:441–449
- Dobrzhinetskaya L, Green HW, Wang S (1996) Alpe Arami: a peridotite massif from depths of more than 300 kilometers. *Science* 271:1841–1845
- Drury MR (1991) Hydration-induced climb dissociation of dislocations in naturally deformed mantle olivine. *Phys Chem Minerals* 18:106–116
- Engi M, Lindsley DB (1980) The stability of titanian clinohumite: experiments and thermodynamic analysis. *Contrib Mineral Petrol* 72:415–424
- Evans BW, Trommsdorff V (1983) Fluorine hydroxyl titanian clinohumite in Alpine recrystallized garnet peridotite: compositional controls and petrologic significance. *Am J Sci* 283A:355–369
- Fujino K, Takeuchi Y (1978) Crystal chemistry of titanian chondrodite and titanian clinohumite of high pressure origin. *Am Mineral* 63:535–543
- Green DH, Falloon TJ (1998) Pyrolite: a ringwood concept and its current expression. In: Jackson I (ed) *The Earth's mantle: composition, structure, and evolution*. Cambridge University Press, Cambridge, pp 311–378
- Green HW, Dobrzhinetskaya L, Riggs EM, Zhen-Ming J (1997) Alpe Arami: a peridotite massif from the Mantle Transition Zone? *Tectonophysics* 279:1–21
- Hermann J, O'Neill HSC, Berry AJ (2005) Titanium solubility in olivine in the system $\text{TiO}_2\text{-MgO-SiO}_2$: no evidence for an ultra-deep origin of Ti-bearing olivine. *Contrib Mineral Petrol* 148:746–760
- Hirth G, Kohlstedt DL (1996) Water in the oceanic upper mantle: implications for rheology, melt extraction and the evolution of the lithosphere. *Earth Planet. Sci Lett* 144:93–108
- Jahn B-M, Fan Q, Yang J-J, Henin O (2003) Petrogenesis of the Maowu pyroxenite-eclogite body from the UHO metamorphic terrane of Dabieshan: chemical and isotopic constraints. *Lithos* 70:243–267
- Jones NW, Ribbe PH, Gibbs GV (1969) Crystal chemistry of the humite minerals. *Am Mineral* 54:391–411
- Karato S, Jung H (1998) Water, partial melting and the origin of the seismic low velocity zone in the upper mantle. *Earth Planet Sci Lett* 157:193–207
- Kincaid C, Sacks IS (1997) Thermal and dynamical evolution of the upper mantle in subduction zones. *J Geophys Res* 102:12295–12315
- Kitamura M, Kondoh S, Morimoto N, Miller GH, Rossman GR, Putnis A (1987) Planar OH-bearing defects in mantle olivine. *Nature* 328:143–145
- Lemaire C, Kohn SC, Brooker RA (2004) The effect of silica activity on the incorporation mechanism of water in synthetic forsterite: a polarised infrared spectroscopy study. *Contrib Mineral Petrol* 147:48–57
- Liou JG, Zhang RY (1998) Petrogenesis of an ultrahigh-pressure garnet-bearing ultramafic body from Maowu. *Isl Arc* 7:115–134
- Lopez Sanchez-Vizcaino V, Trommsdorff V, Gomez-Pugnaire MT, Garrido CJ, Müntener O, Connolly JAD (2005) Petrology of titanian clinohumite and olivine at the high-pressure breakdown of antigorite serpentinite to chlorite harzburgite (Almirez Massif, S. Spain). *Contrib Mineral Petrol* 149:627–646

- Malaspina N, Hermann J, Scambelluri M, Compagnoni R (2006) Polyphase inclusions in garnet-orthopyroxenite (Dabie-Shan, China) as monitors for metasomatism and fluid-related trace element transfer in subduction zone peridotite. *Earth Planet Sci Lett* 249:173–187
- Matsyuk SS, Langer K (2004) Hydroxyl in olivines from mantle xenoliths in kimberlites of the Siberian platform. *Contrib Mineral Petrol* 147:413–437
- McKenzie D, Bickle MJ (1988) The volume and composition of melt generated by extension of the lithosphere. *J Petrol* 29:625–679
- Nimis P, Trommsdorff V (2001) Revised thermobarometry of Alpe Arami and other garnet peridotites from the Central Alps. *J Petrol* 42:103–115
- Ribbe PH (1980) The humite series and Mn-analogs. In: Ribbe PH (ed) *Reviews in Mineralogy, Orthosilicates*, vol 5, pp 231–274, Mineralogical Society of America, Washington
- Risold AC (2001). Formation of oxide inclusions in olivine from garnet peridotites (Central Alps). PhD thesis ETH Zürich, 128 pp
- Risold AC, Trommsdorff V, Grobéty B (2001) Genesis of ilmenite rods and palisades along humite-type defects in olivine from Alpe Arami. *Contrib Mineral Petrol* 140:619–628
- Robinson K, Gibbs GV, Ribbe PH (1973) The crystal structure of the humite minerals. IV Clinohumite and Titanoclinohumite. *Am Mineral* 58:43–49
- Scambelluri M, Müntener O, Hermann J, Piccardo GB, Trommsdorff V (1995) Subduction of water into the mantle: history of an Alpine peridotite. *Geology* 23:459–462
- Scambelluri M, Rampone E (1999) Mg-metasomatism of oceanic gabbros and its control on Ti-clinohumite formation during eclogitization. *Contrib Mineral Petrol* 135:1–17
- Stalder R, Ulmer P (2001) Phase relations of a serpentinite composition between 5 and 14 GPa: significance of clinohumite and phase E as water carriers into the transition zone. *Contrib Mineral Petrol* 140:670–679
- Thompson JB (1978) Biopyriboles and polysomatic series. *Am Mineral* 63:239–249
- Trommsdorff V, Evans BW (1980) Titanian hydroxyl-clinohumite: formation and breakdown in antigorite rocks. *Contrib Mineral Petrol* 72:229–242
- Ulmer P, Trommsdorff V (1999) Phase relations of hydrous mantle subducting to 300 km. In: Fei Y, Berthka CM, Mysen B (eds) *Mantle petrology: field observations and high pressure experimentation: a tribute to Francis R. (Joe) Boyd*. The Geochemical Society, Special publication, pp 259–281
- Weiss M (1997). Clinohumites: a field and experimental study, PhD thesis ETH-Zürich, 168 pp
- Wirth R, Dobrzhinetskaya L, Green HW II (2001) Electron microscope study of the reaction olivine + H₂O + TiO₂ → titanian clinohumite + titanian chondrodite synthesized at 8 GPa, 1300 K. *Am Mineral* 86:601–610
- Yang JJ (2003) Titanian clinohumite-garnet-pyroxene rock from the Su-Lu UHP metamorphic terrane, China: chemical evolution and tectonic implications. *Lithos* 70:359–380